

430 c

DC BIAS DEPENDENT DYNAMIC PROPERTIES OF INJECTION LASERS

DC BIAS DEPENDENT DYNAMIC PROPERTIES OF INJECTION LASERS

by

John C. Goodwin

PART B: McMASTER (OFF-CAMPUS) PROJECT\*

A project report submitted in partial fulfillment of  
the requirements for the degree of  
Master of Engineering

Department of Engineering Physics

McMaster University

Hamilton, Ontario, Canada

1977

\* One of two project reports. The other one is designated PART A:  
ON-CAMPUS PROJECT

MASTER OF ENGINEERING (1977)  
Department of Engineering Physics

McMASTER UNIVERSITY  
Hamilton, Ontario.

**TITLE:** DC Bias Dependent Dynamic Properties of Injection Lasers  
**AUTHOR:** John C. Goodwin  
**SUPERVISOR:** Dr. J.C. Dymont, Bell Northern Research Labs, Ottawa, Ont.  
**NO. OF PAGES:** vi, 45

## ABSTRACT

It was observed that the spontaneous carrier lifetimes of GaAlAs injection lasers, as measured by the time delay method, exhibit a strong dependence on the DC bias current flowing through the laser. As the DC bias current is increased, the measured lifetimes decrease, passing through a minimum at bias currents less than 0.1 mA, and then rise again to an intermediate value at high bias currents. It was also found that the impedance of these lasers to fast current pulses drops sharply at the same DC bias currents as the minimum measured lifetime mentioned above. Evidence is presented to suggest that both of these effects are due to an electrical resonance between the stray drive circuit inductance and the DC bias dependent capacitance of the laser's junction under forward bias.

In addition, two methods of determining the spontaneous carrier lifetime by other than the time delay method are described. One method involves measurement of the vector impedance of lasers to sinusoidal drive currents at frequencies less than 100 MHz, as a function of DC bias. The second method is based upon the frequency dependence of the phase shift between a sinusoidal drive current and the resulting spontaneous light.

### Acknowledgements

The author would like to thank Bell Northern and especially Dr. J.C. Dymont for the opportunity to do this project, and Dr. J. Straus for his suggestions regarding equipment.

## TABLE OF CONTENTS

	<u>Page</u>
ABSTRACT	iii
ACKNOWLEDGEMENTS	iv
LIST OF ILLUSTRATIONS	vi
CHAPTER 1: INTRODUCTION	1
CHAPTER 2: DC BIAS DEPENDENT DYNAMIC PROPERTIES	4
CHAPTER 3: CAPACITANCE MEASUREMENT	
3.1 Experimental Procedure	18
3.2 Analysis of Data	29
3.3 Discussion of Capacitance Measurements	35
CHAPTER 4: RADIO FREQUENCY VECTOR DRIVE EFFICIENCY EXPERIMENT	
4.1 Theory and Experimental Procedure	37
4.2 Discussion of RF drive efficiency results	41
CHAPTER 5: CONCLUSIONS	43
REFERENCES	45

## LIST OF ILLUSTRATIONS

<u>Figure</u>		<u>Page</u>
1	Time Delay Plots for Laser 289/1 by J.C. Dymant	5
2	Bias Insertion/Drive Circuit for Injection Lasers	7
3	Calculated Carrier Lifetimes for Laser 289/2	10
4	Relative Impedance of Laser 289/2	13
5	Simplified Equivalent Circuit of Injection Laser or LED	15
6	Impedance Magnitude vs. $I_{DC}$ for Laser 289/2	19
7	Impedance Magnitude vs. $I_{DC}$ for LED 42/45	22
8	Impedance Phase Angle vs. $I_{DC}$ for LED 42/45	23
9	Oxide Stripe Geometry Double Heterostructure Laser	26
10	I-V Characteristics of LED 42/45	27
11	Calculated Capacitance of LED 42/45 as a Function of DC Bias	33

CHAPTER 1  
INTRODUCTION

In semiconductor lasers, there is a time delay between the application of a current pulse to the laser and the onset of stimulated emission. This time delay is due to the fact that a finite amount of time is needed to create the population inversion necessary for lasing. The time delay decreases as the inversion is pumped harder, i.e. as the driving current pulse is taken farther above the laser's threshold current.

For a fixed current pulse amplitude, the time delay can be reduced by DC biasing the laser at a substantial fraction of the threshold current. The dependence of the time delay on the DC bias can be shown to be<sup>(1)</sup>

$$t_d = \tau_{sp} \ln \left( \frac{I - I_{DC}}{I - I_{th}} \right) \quad (1)$$

where  $I$  is the total current (DC bias plus drive pulse)

$\tau_{sp}$  is the spontaneous lifetime of the injected carriers

$t_d$  is the resulting time delay

Typical  $\tau_{sp}$  values are of the order of two nanoseconds.

To modulate injection lasers at Gbit rates or more it is necessary to have time delays much less than one nanosecond. From (1), it can be seen that very small time delays are obtained when  $I_{DC}$  is close to  $I_{th}$ .

The conventional method of measuring  $\tau_{sp}$  is to measure the time delays as the current pulse amplitude is varied, and then to fit the data to the expression given above. As was mentioned earlier, the  $\tau_{sp}$  values determined by this method were observed to go to a sharp minimum at a critical  $I_{DC}$ . This critical bias was on the order of 0.1 mA, much less than the threshold currents which are on the order of 100 mA. At this same time, it was also noticed that the laser's impedance to fast current pulses dropped sharply at the critical  $I_{DC}$ . If slower rise time pulses were used, the critical bias current shifted to a higher value.

It has been already observed by J.C. Dymant that the time delays are sensitive to the device capacitance. Under the DC forward bias used, some of the device capacitance would be due to diffusion capacitance at the junction. As shown by Sze<sup>(2)</sup>, diffusion capacitance will increase with  $I_{DC}$ . It is thought that the capacitance of the device slows the response of the junction to a fast current pulse so that the measured time delays imply a larger  $\tau_{sp}$  value than is actually true. One mechanism by which this might occur is that the device capacitance, especially the component due to the metal contacts, rounds out the rising side of the current pulse as it reaches the junction.

If there is an electrical resonance between the device capacitance and a series inductance, the increase in signal across the device capacitance may enhance the rising side of the current pulse that reaches the junction so as to compensate for the rounding effect. The device capacitance will depend on the DC bias applied. For this reason, the resonance point could follow the critical  $I_{DC}$ , depending on the

rise time of the current pulse. The series inductance is just the stray inductance due to the connecting wires. Since this is fixed, a more slowly rising current pulse would require a larger capacitance, to be found at a higher  $I_{DC}$ , to resonate with the lower frequencies associated with the longer risetime.

Further investigation was required to verify the electrical resonance explanation of the  $\tau_{sp}$  minimum and to determine how  $\tau_{sp}$  should be measured in view of its DC bias dependence using the time delay method.

The main body of this report will be divided into three chapters. The first of these, entitled "DC bias dependent dynamic properties" will present the detailed evidence leading to the electrical resonance explanation. The next chapter is concerned with the capacitance measurements done on lasers and LED's. The initial purpose of this was to verify the electrical resonance by knowing the device capacitance as a function of forward bias. As well, since the diffusion capacitance is a function of  $\tau_{sp}$ , it was thought that an independent value of  $\tau_{sp}$  could be found from the frequency dependence of the diffusion capacitance. The final chapter of the main body discusses a drive efficiency experiment. During the capacitance measurement evidence appeared to suggest that the drive efficiency of lasers and LED's may peak near the critical  $I_{DC}$ . The drive efficiency at radio frequencies (R.F.) was measured as a function of  $I_{DC}$  in order to verify this. As well, it should be possible to determine  $\tau_{sp}$  from the frequency dependence of the phase shift between the driving current and the resulting spontaneous light.

## CHAPTER 2

### DC BIAS DEPENDENT DYNAMIC PROPERTIES

As mentioned earlier, the dynamic characteristics of injection lasers which are reported here were first noticed in the amplitudes of fast current pulses through various lasers. Following common procedure when applying fast current pulses through 50  $\Omega$  cable to laser diodes, the lasers were put in series with a 47  $\Omega$  resistor and had a DC bias current flowing through them. A schematic diagram of this biasing arrangement is shown in Figure 1. The purpose of the DC bias is to insure that the dynamic resistance of the laser diode is always down to a few ohms or less. If the laser diode is in series with a 47  $\Omega$  resistor, then the combination will always be matched in impedance to the 50 ohm cable which supplies the pulse. This is necessary to prevent reflection of the current pulse off the end of the mismatched cable.

When this dependence of the current pulse amplitude on the DC bias was first noticed, it was thought that the applied DC bias was not sufficient to put the laser diode into its low dynamic resistance state. This seemed to correlate with the fact that increasing the DC bias beyond a few milliampères had no further effect on the current pulse amplitude. However, if this were the case, the current of the pulse itself would have put the diode into the low resistance state after a few nanoseconds or so. We would then have found that the current after this time would be independent of the DC bias. Instead, the entire plateau of the current pulse increased in amplitude as the DC bias was

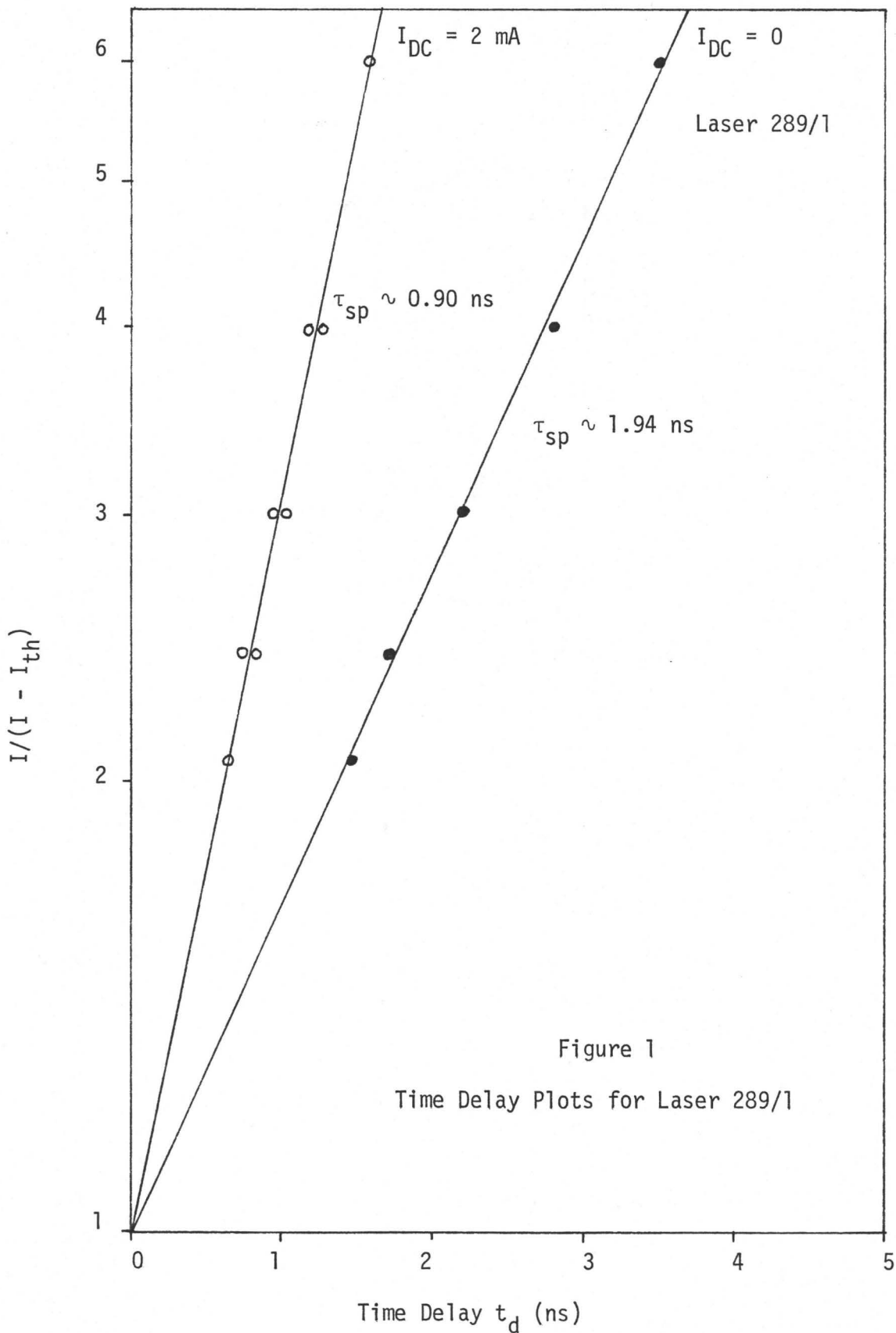
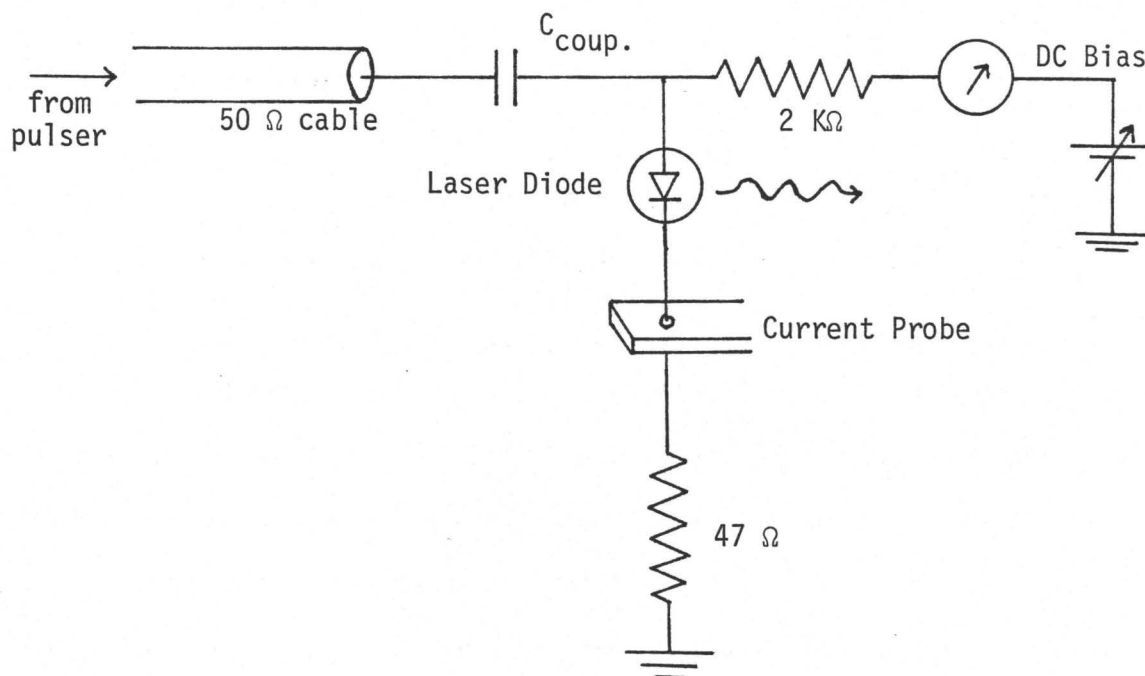


Figure 1  
Time Delay Plots for Laser 289/1

increased. Another argument against this explanation is that the dynamic resistance of these lasers isn't down to 3 ohms until 10-20 mA of DC bias are applied, rather than the few mA that was initially assumed.

At the same time as this effect appeared, Dr. Dymant noticed that the time delay measurements that he made on various lasers had a dependence on the DC bias current that was much stronger than the theory predicts. These measurements are the means by which the spontaneous carrier lifetimes of the lasers are typically measured. The DC bias current, current pulse amplitude and the resulting time delay of the stimulated light are measured. The threshold current of the laser being measured is known, and so the quantity inside the round brackets of expression (1) may be calculated. A semi-log plot is made of the time delays that are measured against the corresponding calculated current quantities. The slope of a straight line drawn through the data points yields the  $\tau_{sp}$  value. The resulting line will not necessarily pass through the origin of the plot. This is because no provision is made to synchronize the light trace and the current trace on the oscilloscope screen from which the measurements are made. This does not present a problem since it is only the slopes of the lines that are significant.

As is shown in Figure 2, the time delay data measured by Dr. Dymant followed a straight line for both the  $I_{DC} = 2$  mA case and the  $I_{DC} = 0$  mA case. However, the slope of the line for  $I_{DC} = 2$  mA corresponded to a spontaneous lifetime which is less than half of that of the  $I_{DC} = 0$  mA line. Dr. Dymant suggested that this could be due to the capacitance of the device changing with DC bias. Further work was needed to determine which value of bias produced the true spontaneous



$C_{coup}$  - this coupling capacitor passes the current pulses from the pulser to the laser diode while blocking the DC bias current from the pulser - for pulses longer than a few  $\mu\text{s}$ ,  $C_{coup}$  should be a few  $\mu\text{f}$  or more to keep the pulse top flat.

#### Current Probe

- the current pulse through the laser was monitored with either a Tektronix CT - 1 current probe (5 mV/mA sensitivity) or a Tektronix CT-2 current probe (1 mV/mA sensitivity).

Figure 2

lifetime.

The EH125A pulser which was used in the time delay measurements was limited in output to only 200 mA through 50  $\Omega$ . To produce a wide spread in the time delay data with low  $I_{DC}$ , it would be useful to employ current pulses up to  $2 I_{th}$ . This limits the choice of lasers available for characterization to those with  $I_{th} = 100$  mA or less. The only lasers available that fall into this category were some of the 3 mil long pieces, as opposed to the usual 13 mil pieces.

Lasers 289/5 and 289/2 were selected for investigation. Laser 289/5 had a sluggish turn-on for the stimulated light, so 289/2 was used exclusively. By observing the rate of increase in the photo-current amplitude as the drive pulse amplitude was increased, the 289/2's threshold current was determined to be  $I_{th} = 75$  mA  $\pm$  3 mA.

Time delay runs were done on 289/2 for a series of  $I_{DC}$  values between 0 mA and 7 mA. Taking  $I_{DC} = 75$  mA, plots were made of the time delays using the measured  $I_{DC}$  and drive pulse amplitude ( $I_p$ ) values. It was noticed that for some  $I_{DC}$  values, i.e.  $I_{DC} = 0.1$  mA, the time delay points curved upwards at the right hand side of the plot instead of continuing along on the expected straight line. It was thought that since the long time delay points on the plot corresponded to  $I_p$  values close to  $I_{th}$ , that a slight error in  $I_{th}$  could cause a large error in the right hand side of expression (1). If the  $I_{th}$  value used was larger than the actual value, the plot should curve upwards on the right hand side. To verify this, the time delays for  $I_{DC} = 0.1$  mA were re-plotted taking  $I_{th} = 73$  mA, and then  $I_{DC} = 70$  mA. Even at  $I_{th} = 70$  mA, the data points still curve upwards on the right, although

to a lesser extent than before. However,  $I_{th}$  was measured to be 75 mA  $\pm$  3 mA. The actual value couldn't have been as small as 70 mA without being noticed in the initial threshold measurement.

One possible cause of the curvature of the data points is that the derivation of expression (1) assumes square current pulses rather than pulses whose risetime is a significant fraction of the time delays, as is the case with our measurements.

This pattern of curvature of the data points isn't consistent at all  $I_{DC}$  values. For instance, the points at  $I_{DC} = 0$  mA curve downward at the right hand side for both  $I_{th} = 70$  mA and  $I_{th} = 75$  mA. The time delay points for  $I_{DC} = 30$   $\mu$ A form a fairly straight line for both  $I_{th} = 70$  mA and  $I_{th} = 75$  mA, although the slopes and intercepts change.

For all  $I_{DC}$  values, if the right hand side of the plots is ignored, straight lines can be fitted fairly well to the left hand side. The  $\tau_{sp}$  values calculated from the slopes of the lines show that the apparent spontaneous carrier lifetime is less at 2 mA than at 0 mA. This is what Dr. Dymont reported on a similar laser. However, here the calculated lifetimes go to a minimum at  $I_{DC} = 30$   $\mu$ A, as is shown in Figure 3. To identify the cause of this anomalous behaviour, various properties of the laser were investigated as a function of DC bias.

An I-V curve was plotted for laser 289/2, with a high density of points taken near  $I_{DC} = 30$   $\mu$ A. Dynamic resistances were calculated from the slopes of tangents to this curve. No anomalous behaviour appeared in the dynamic resistance near  $I_{DC} = 30$   $\mu$ A.

Next, the capacitance of laser 289/2 was measured as a function of DC bias. This was suggested by Dr. Dymont because he had noticed

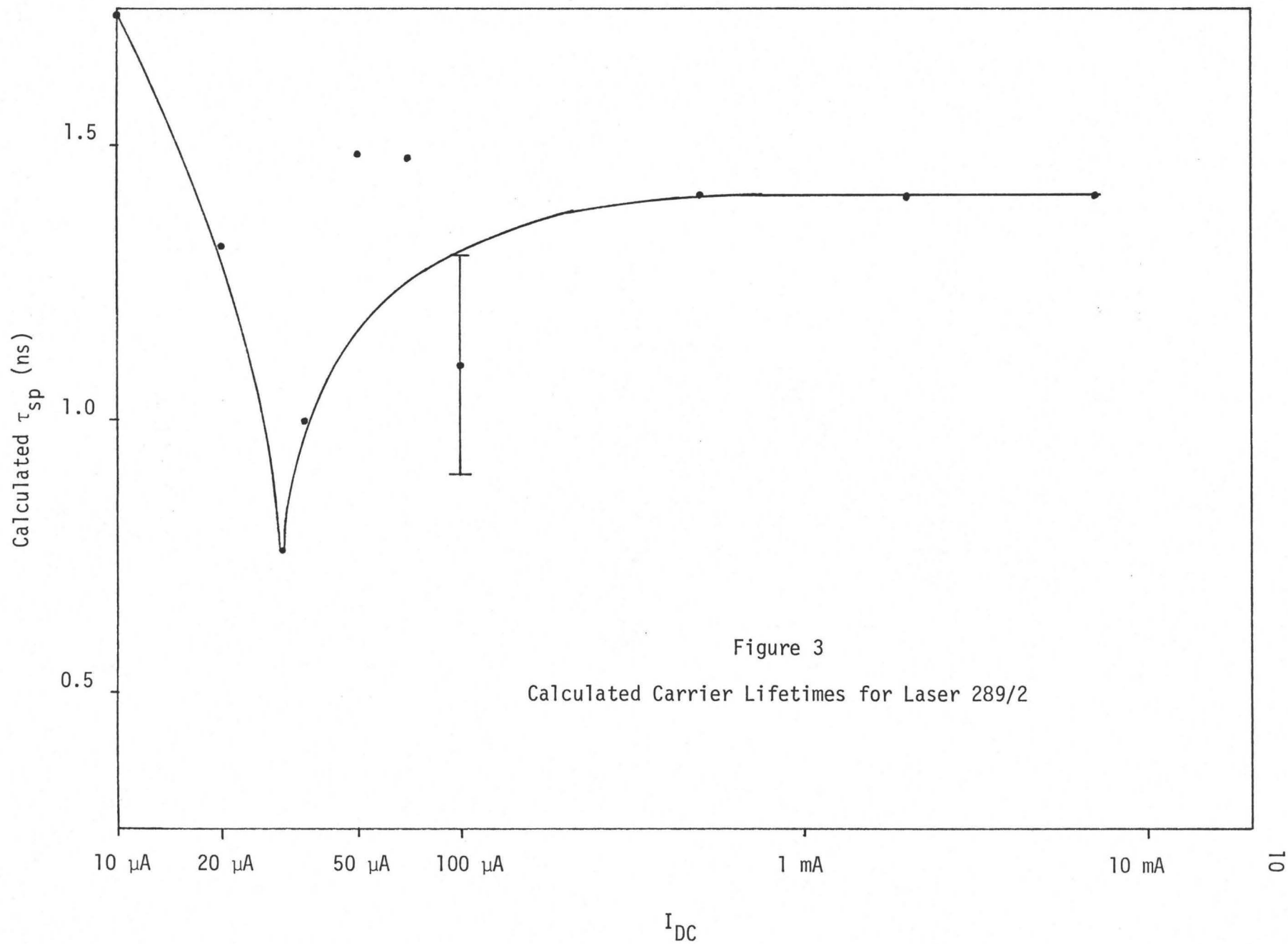


Figure 3

Calculated Carrier Lifetimes for Laser 289/2

smaller time delays for proton bombarded devices, which are known to have smaller capacitance than the oxide stripe lasers which were being used here. This measurement was done with a Boonton model 71A capacitance meter. Laser 289/2 was observed to have a capacitance which increased steadily with  $I_{DC}$ , exhibiting no strange behaviour near  $I_{DC} = 30 \mu\text{A}$ . This was done up to  $I_{DC} = 0.8 \text{ mA}$ . The capacitance was on the order of 100 pf in this range of  $I_{DC}$ .

Laser 7/5, a 13 mil long laser, had capacitances that were larger than those of the 289/2 at the same  $I_{DC}$  values. This is expected because of 7/5's larger area. However, the 7/5 capacitance was observed to rise with  $I_{DC}$ , peak at about 460 pf near  $I_{DC} = 100 \mu\text{A}$ , and then decrease again. At  $I_{DC} = 2.0 \text{ mA}$ , it was found that there was poor carry-over between different scales on the capacitance meter. For example, the 7/5 was measured to have 18/pf on the 1000 pf scale at  $I_{DC} = 2.0 \text{ mA}$ , but on the 300 pf scale the needle was well off the upper end. This carry-over problem did not exist at lower  $I_{DC}$ .

This same behaviour had been noticed earlier when the Boonton meter was being used to measure the stray capacitance of various resistors. Stray capacitances of less than 1 pf were expected, but a  $220 \Omega$  resistor measured 81 pf on the 1000 pf scale, and off scale on the 100 pf scale. As the resistances got larger, the measured capacitances decreased and the carry-over problem became less pronounced, but never disappeared. It was thought that the same thing might happen with a laser diode. The Boonton meter puts a 1 MHz signal through the device to be tested, to measure its capacitance. At 1 MHz, it was thought that as the junctions dynamic resistance decreased as

$I_{DC}$  was increased, it would start to shunt the junction's capacitance. The laser would then start to look like a resistance, and it would be reasonable to expect behaviour similar to that encountered when measuring the stray capacitance of a resistor.

According to R.E. Lafferty of Boonton Electronics, the model 71A capacitance meter will not operate properly for devices with parallel resistance and Q factors of about three or less. Apparently the phase detector in the 71A is unable to detect the capacitive component of the signal from the device if the resistive component is above a certain relative magnitude.

Laser 7/5 has a dynamic resistance of about  $2\text{ K}\Omega$  at  $I_{DC} = 100\ \mu\text{A}$ . For a capacitance of about  $400\text{ pf}$  at  $1\text{ MHz}$ , the reactance is about  $400\ \Omega$ . Defining Q by the admittance ratio, this corresponds to a Q of 5. This may be the cause of the peak in the Boonton meter's capacitance reading. We expect diffusion capacitance to dominate in this current range and so the capacitance should increase steadily with  $I_{DC}$ . Perhaps the decrease in capacitance above  $100\ \mu\text{A}$  is due to exceeding the Q limit of the capacitance meter. At any rate, the capacitance of 289/2 had no strange behaviour near  $I_{DC} = 30\ \mu\text{A}$ .

Another property of the 289/2 that was investigated near  $I_{DC} = 30\ \mu\text{A}$  is the impedance of the laser to fast current pulses. The output pulse amplitude of the EH125A pulser that was used is fixed internally. To adjust the pulse amplitude which is applied to the laser,  $50\ \Omega$  variable attenuators were inserted after the pulser. The attenuators after the EH125A were set to a certain point, and the amplitude of the current pulses going through the laser were measured as a function of the DC

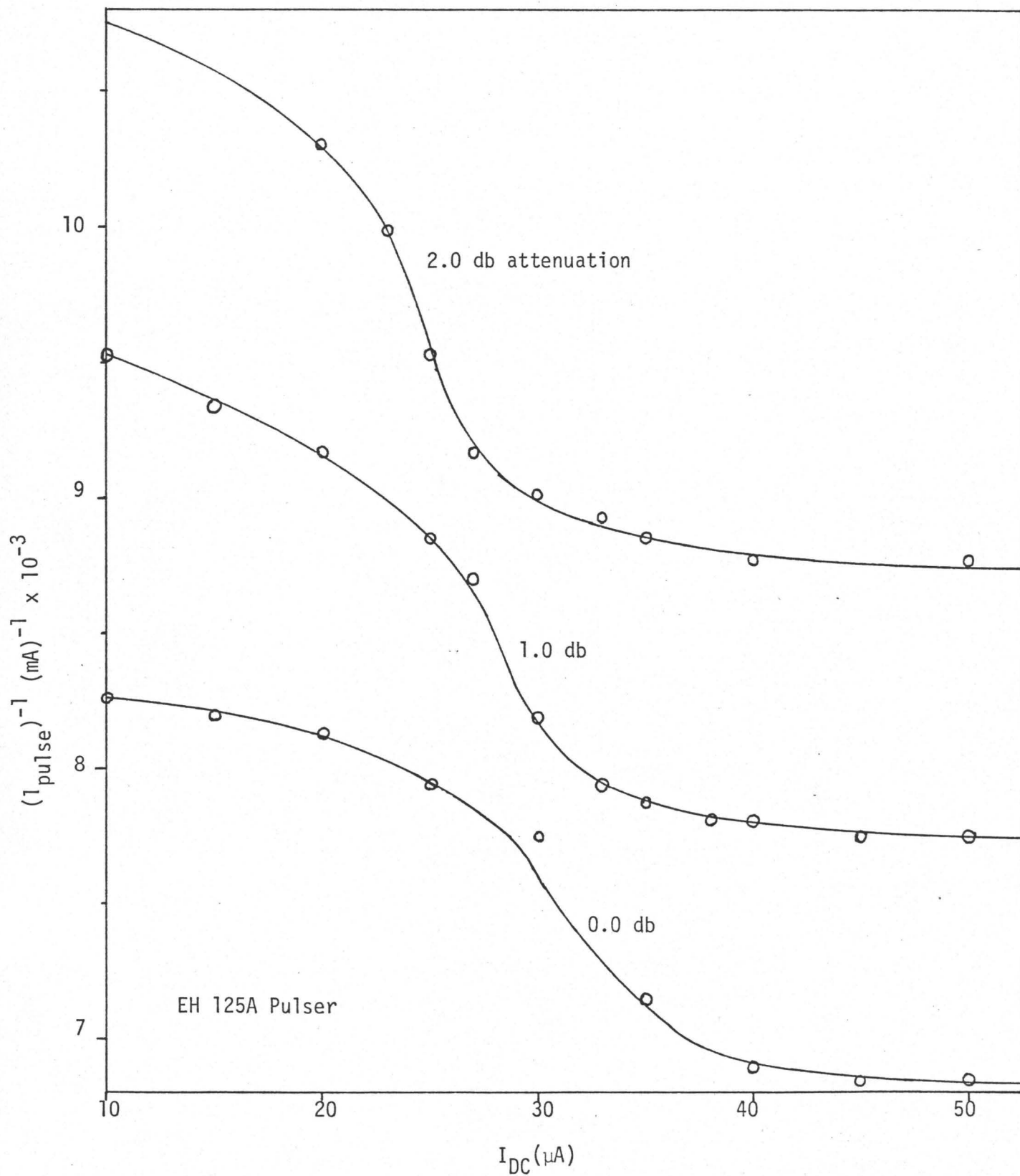


Figure 4

Relative Impedance of Laser 289/2 (3 mil piece)

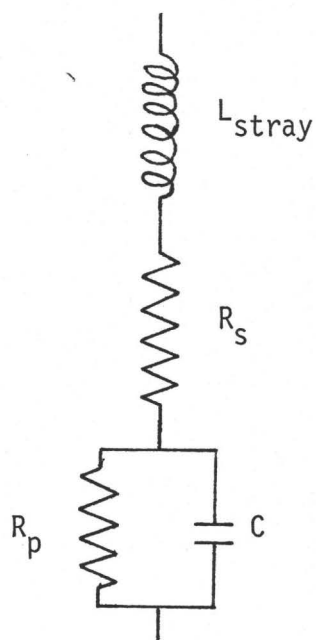
bias applied. In Figure 4 the reciprocal of the current pulse amplitude is plotted against  $I_{DC}$  for various attenuator settings.

As can be seen from this plot, the "relative impedance" (of laser plus  $47 \Omega$  resistor plus pulser output resistance) starts out flat, drops near  $I_{DC} = 30 \mu A$  and then levels out at high  $I_{DC}$ . As more attenuation is introduced, the inflection point shifts to lower DC currents and seems to develop a sharper curve. It appears that although this laser's capacitance and dynamic resistance exhibit no strange behaviour near  $I_{DC} = 30 \mu A$ , the impedance of the laser to these current pulses changes rapidly here.

To investigate this effect further, the same experiment was performed with a different pulser having a slower risetime. The risetime of the current pulses from the EH125A pulser into the circuit containing laser 289/2 was less than one nanosecond. The HP214A which was later used had a current pulse risetime of a few nanoseconds. The behaviour of the "relative impedance" was the same as for the other pulser except that now the inflection point is near  $I_{DC} = 100 \mu A$ .

At this higher  $I_{DC}$ , we expect the junction capacitance to be greater. The more slowly rising current pulse from the HP214A would have lower frequency components in its Fourier transform than would the EH125A's pulses. This, plus the fact that the time delays and relative impedance change so sharply with  $I_{DC}$ , suggests the following explanation.

A simple equivalent circuit model of the laser diode and associated circuitry is shown in Figure 5. For the purpose of this analysis, the pulser output resistance,  $47 \Omega$  resistor and laser diode bulk series resistance (typically a few ohms) can be grouped into one series resis-



$L_{\text{stray}}$  - stray circuit series inductance

$R_s$  - bulk series resistance of device, plus any series circuit resistance i.e. pulser output resistance or  $47 \Omega$  impedance matching resistor

$C$  - device capacitance, mostly due to junction properties

Figure 5

Simplified Equivalent Circuit of Injection Laser or LED

tance. If the stray series inductance is of the order of 100 nanohenries, then the response of the laser to these fast current pulses would be greatly affected. This is because a large fraction of the higher frequency components of the applied voltage pulse would be dropped across the inductance. The diffusion capacitance of the junction will increase with  $I_{DC}$ . Therefore, at a certain  $I_{DC}$  value, the total capacitance of the laser and the stray inductance will form a series resonant circuit for the high frequencies that exist at the front of the current pulse. At this series resonance, the current contribution of these frequencies would go to a maximum. The front of the pulse should then be enhanced at this critical  $I_{DC}$  value. T.P. Lee<sup>(3)</sup> has reported considerable reduction in time delays by using an RC network to enhance the front of the drive pulse.

The pulses from the HP214A would have a lower risetime characteristic frequency than those of the EH125A. For a fixed  $L_{stray}$ , the series resonance should then occur at a higher capacitance, i.e. at a higher  $I_{DC}$  value. This is what was observed.

Presumably, if the series resistance in the circuit could be reduced, the Q at resonance would be greater. We might then expect a greater enhancement of the front of the pulse, and shorter time delays. This could easily be done with existing equipment by shunting the drive circuit with a low resistance to reduce the effective source resistance from 50  $\Omega$ . The 47  $\Omega$  series resistor would then be correspondingly reduced. This was not done because the current pulses from the EH125A are already limited in amplitude. The effective source resistance wouldn't be changed very much before so much current is lost through

the shunt that the pulse reaching the laser couldn't get up to  $I_{th}$ .

To be able to verify this resonance explanation quantitatively, it is necessary to know the stray inductance, and the junction capacitance and resistance as a fraction of frequency and DC bias.

Up to this point, the junction's dynamic resistance had been determined by the slope of the I-V curve of the device. However, due to the finite accuracy and resolution of the instruments being used, this method is not very accurate. This is especially true at the higher DC biases where the junction voltage is approaching saturation. A direct method of determining the dynamic resistance would then be better than this differential method.

For measuring the capacitance easily as a function of  $I_{DC}$ , the Boonton capacitance meter would be ideal. However, low Q problems at 1 MHz appear to ruin the measurement for all but the lowest DC biases. A similar instrument operating at 10 MHz may solve the problem since the device Q's would then be higher.

One alternative method of measuring the laser's capacitance is to use an AC bridge. Another method would be to put the laser in series with a known inductance, and look for the resonances of an applied RF wave that is swept in frequency. Both of these methods were tried, but neither proved satisfactory.

## CHAPTER 3

### CAPACITANCE MEASUREMENT

#### 3.1 Experimental Procedure

To measure the lasers capacitance under forward bias, the method that was finally used involved a vector impedance meter (HP4815A) which is capable of operating at up to 100 MHz. These high frequencies are necessary to raise the Q of the device enough for accurate capacitance measurements to be made. One drawback of using such frequencies is that stray reactive effects in components, etc. could cause significant perturbations - these must be accounted for.

The 4815A displays meter readings of impedance magnitude and phase angle. There are also chart recorder outputs available for the two meters. By using two X-Y recorders, it is possible to simultaneously produce plots of impedance magnitude vs frequency for set values of  $I_{DC}$ , and of impedance phase angle vs frequency. Plots can also be made at fixed frequencies, and sweeping in  $I_{DC}$ . A ten-turn variable current source (HP6177B) was used to supply the sweep in  $I_{DC}$ .

A series of runs on #289/2 was done at various fixed frequencies up to 100 MHz and sweeping in  $I_{DC}$  from 0 mA to 4 mA. As can be seen in Figure 6, there are pronounced "bellies" in the impedance magnitude plots. It is believed that these "bellies" are due to the same electrical resonance as are the time delay minima. The fact that we now see them at much higher  $I_{DC}$  is due to the lower frequencies used here than are associated with the current pulses used in making the time delay measure-

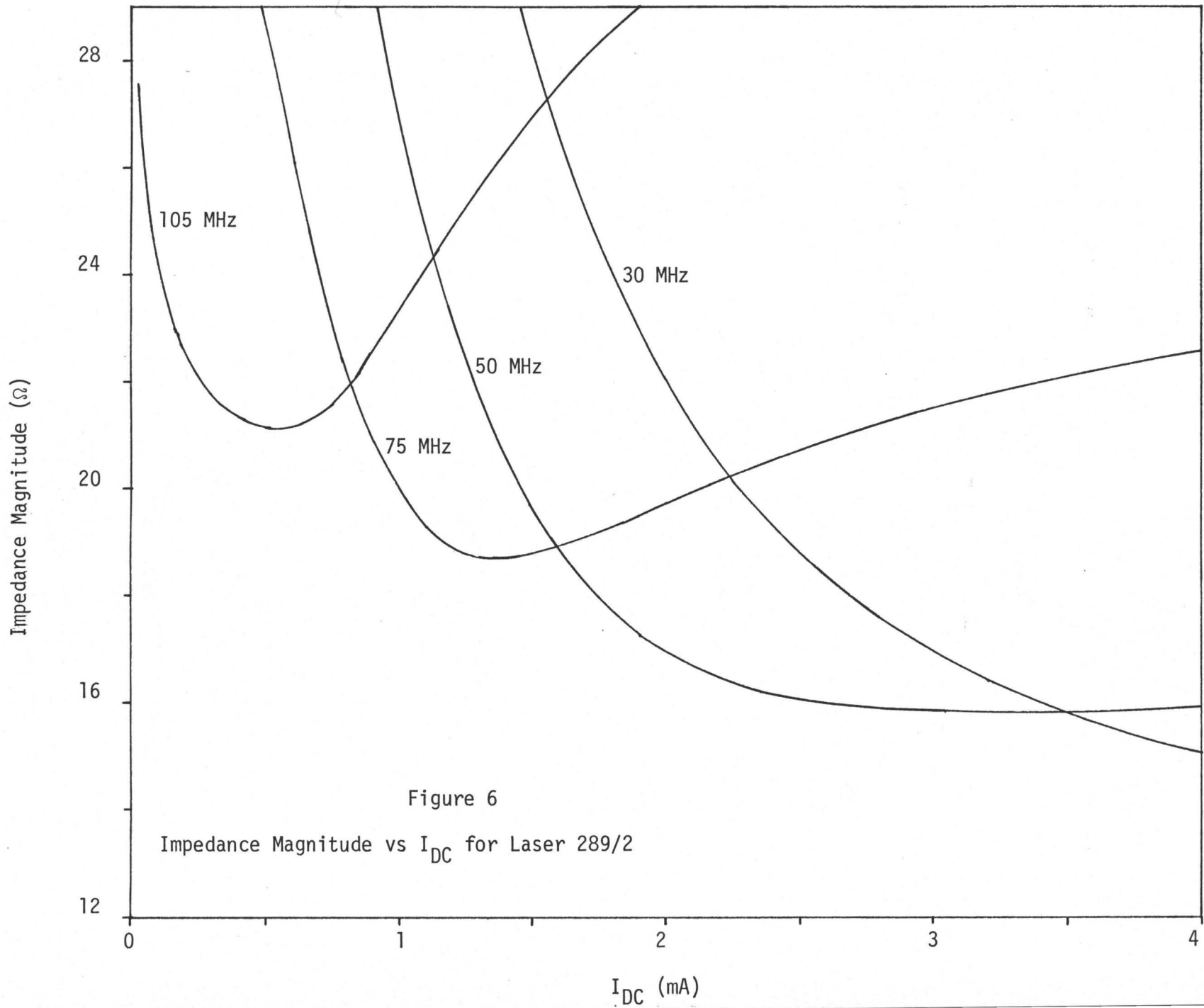


Figure 6  
Impedance Magnitude vs I<sub>DC</sub> for Laser 289/2

ment. More capacitance (at higher  $I_{DC}$ ) is needed to resonate with fixed  $L_{stray}$ . From the plot, we see that the higher frequency runs have their bellies at lower  $I_{DC}$ . This is what we would expect of the series resonant model.

The belly impedances at a couple of mA bias are on the order of 20  $\Omega$ . From the I-V curve for 289/2, the dynamic resistance in this range is closer to 40  $\Omega$  or 50  $\Omega$ . The reactive effects are becoming dominant at these frequencies and can be expected to be even more so for the current pulses from the EH125A.

To measure the reactive effects of the device, we must know what stray circuit reactances the impedance meter is also measuring. The stray series inductance was measured by replacing the 289/2 laser in its ball package mount with an empty ball package. The ball on this package was lowered until it touched the mount, causing a short circuit. The measured impedance is then assumed to be due to the series inductance and the effect of the probe. After accounting for probe effects, this inductance was found to be about 45 nanohenries (nH).

The stray circuit capacitance shunting the laser was measured by raising the ball of the empty package off the mount, and leaving it open. After accounting for probe effects, the shunt capacitance was found to be about 7.5 pf.

According to the 4815A manual, the effect of the probe is to cause an inductance of 8 nH and a resistance of 0.5  $\Omega$  to be in series with the device being measured. The probe also puts 0.3 pf across the device.

After this initial impedance run, other devices were tested to

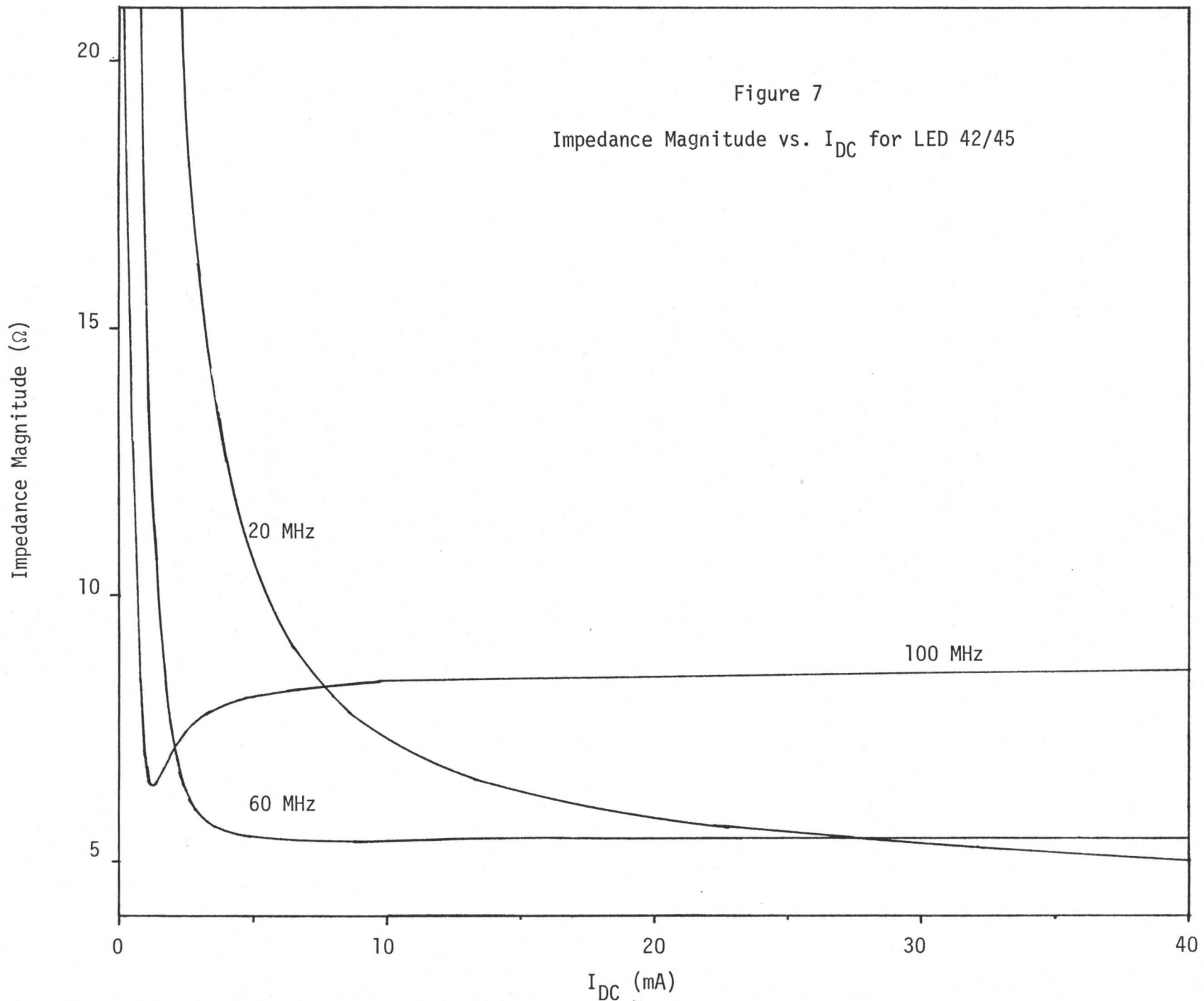
see if the same effects appeared. A 13 mil long laser (#6B/19) was investigated, and it also has a similar series of impedance bellies. It was pointed out that the impedance phenomena being observed should be common to both LED's and lasers. LED #SB42/45 was obtained and it also showed impedance bellies. However, the stray reactances couldn't be measured for the LED configuration. Unlike the loose laser chips in the ball packages, the LED crystal is bonded in and cannot be removed from the mount. In any case, the stray reactances are expected to be of the same order as for the laser chips.

If these phenomena are due to a resonance with the series inductance, then we would expect the impedance behaviour to change if the inductance was reduced. The lowest inductance geometry that could be designed for the LED measurements was simply to bridge the centre pin and ground wire of the impedance meter probe with the leads of the LED package.

In runs done on SB 42/45 in this low inductance geometry, bellies were seen only for frequencies above 60 MHz. Another LED (#44/10) was tested, and showed no bellies at all below 100 MHz.

Because these LED's can safely be driven at DC currents approaching 100 mA when an attachable heat sink is being used, further investigation concentrated on LED's rather than lasers.

In an impedance run done with LED 42/45 up to  $I_{DC} = 50$  mA, it was noticed that the magnitude plot levelled off at high  $I_{DC}$ . At high  $I_{DC}$ , the junctions dynamic resistance and capacitive reactance will be much less than the reactance due to the stray inductance. Figure 7 shows the level portion of the impedance magnitude where the inductance is



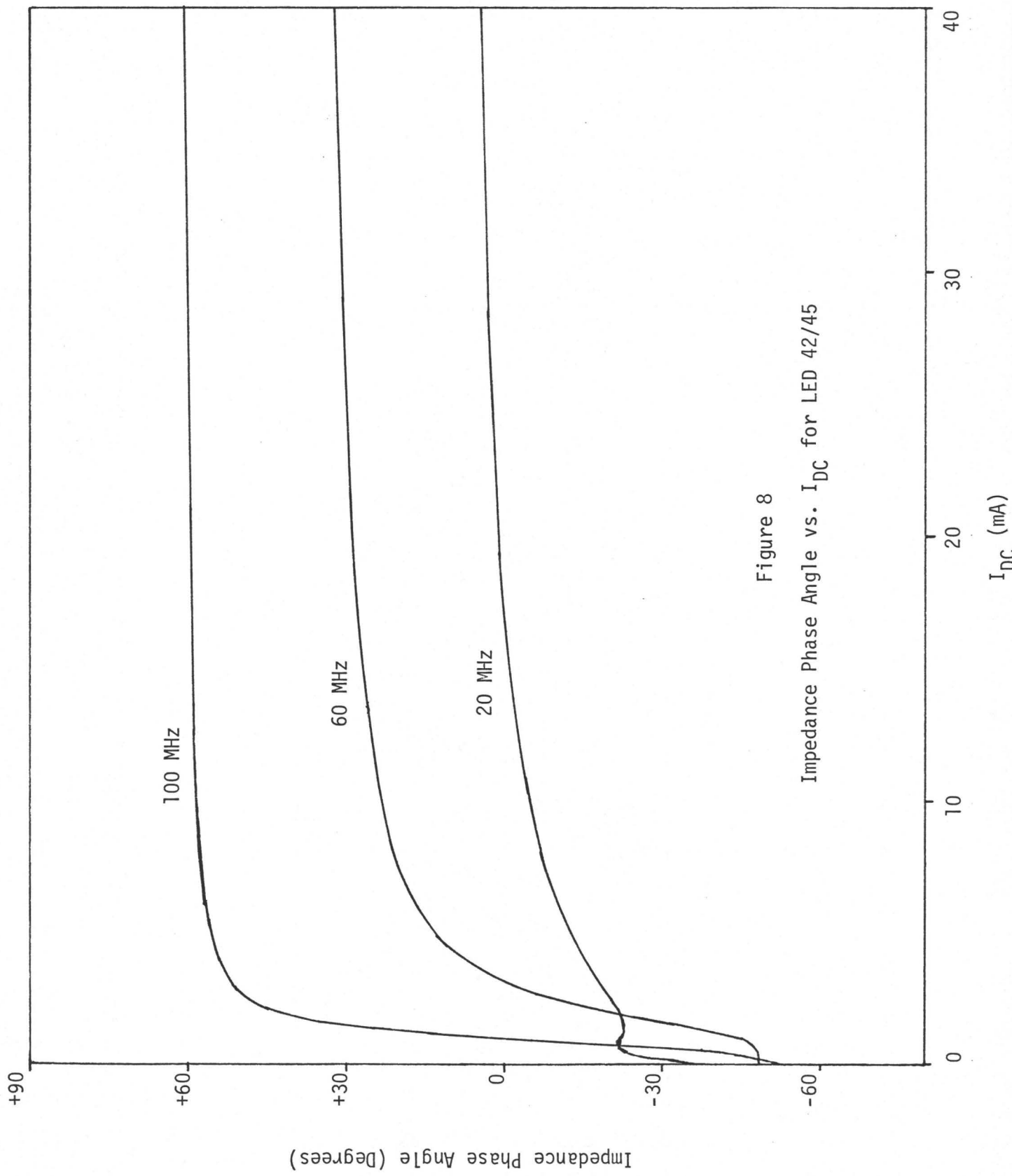


Figure 8  
Impedance Phase Angle vs.  $I_{DC}$  for LED 42/45

Impedance Phase Angle (Degrees)

$I_{DC}$  (mA)

dominant. Figure 8 shows that the inductance also causes the phase to level off at a high positive value. This same behaviour was observed in other LED's and lasers.

The stray inductance of the circuit containing the LED in its package can now be found from the high  $I_{DC}$  plateau in impedance magnitude and phase. For instance, at  $I_{DC} = 50$  mA, the impedance of the 100 MHz run of SB 42/45 in the low inductance configuration has levelled off at  $|Z| = 8.6 \Omega$  and  $\theta = 61^\circ$ . This corresponds to a series inductance of about 4 nH, after accounting for the probe effects.

The expression for the impedance of the circuitry shown in Figure 1 can be shown to be:

$$Z = R_s + \frac{R_f}{1 + (\omega R_p C)^2} + j[\omega L - \frac{\omega R_p^2 C}{1 + (\omega R_p C)^2}] \quad (2)$$

where  $R_p$  is the dynamic resistance of the junction

$C$  is the device capacitance (mostly due to junction properties)

$R_s$  is the bulk series resistance of the device, plus any series resistance in the circuit.

These quantities will also include the effects of the impedance meter probe when impedance measurements are being done.

If the driving frequency is high enough that  $(\omega R_p C)^2 \gg 1$ , then the expression reduced to:

$$Z = R_s + j[\omega L - \frac{1}{\omega C}]$$

It is expected that this will hold true for the frequencies encountered at the front of the EH125A pulses. This expression is clearly that of

a series resonant circuit.

The series resonant condition, at any frequency, is when the imaginary component of the impedance goes to zero i.e. the impedance phase angle is zero. It can be seen from the plots that the impedance bellies always occur at  $I_{DC}$  values above those of the impedance phase zeroes. This is because the junction's dynamic resistance will be a significant shunt to the junction's capacitance at the frequencies and biases near the observed bellies. This will result in a low Q factor at resonance.  $R_p$  is dropping rapidly with  $I_{DC}$  in this region. The low Q and the fact that  $R_p$  will then have decreased considerably across the resonant half-width, could result in this positioning of the impedance bellies.

As Sze points out, diffusion capacitance will be significant under forward bias conditions. He also suggests that  $C_{diff}$  should be proportional to  $I_{DC}$ , since both vary as  $\exp(qV/nkT)$ . This may not be true in the case of oxide stripe heterostructure lasers and Burrus type LEDs. The reason for this is that we expect the size of the working junction to vary with  $I_{DC}$ . It can be seen from Figure 9 that the junction resistance of a laser at very low  $I_{DC}$  would be greater than the spreading resistance of the confining layers. We can then expect the current through the active layer to be more or less evenly distributed over the area of the chip. As  $I_{DC}$  increases, the junction resistance will decrease and eventually will become less than the p confining layer spreading resistance. When this occurs, the current should flow through the active layer only in the region under the stripe contact.

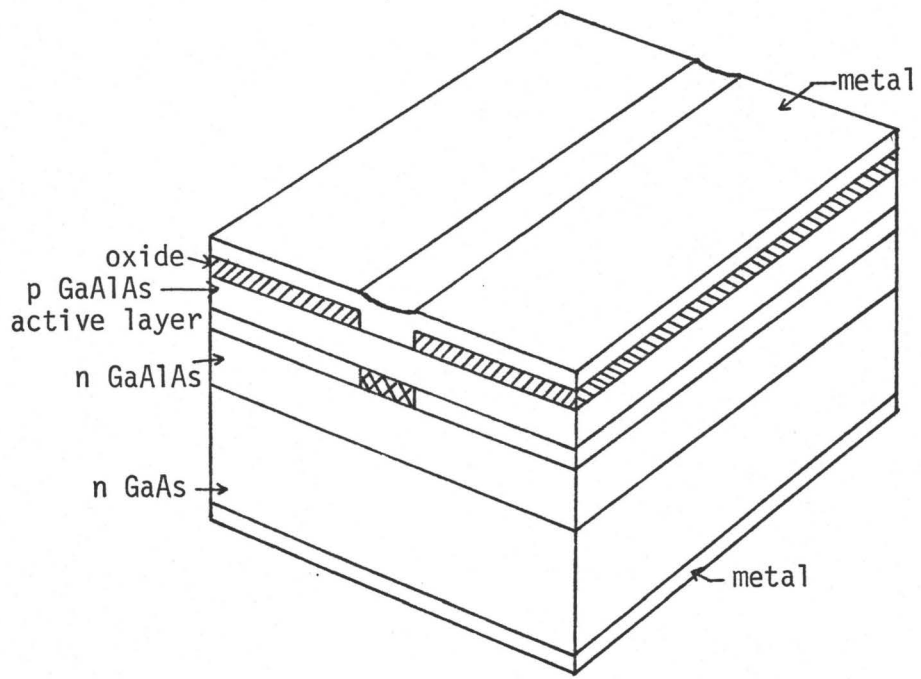


Figure 9

Oxide Stripe Geometry Double Heterostructure Laser

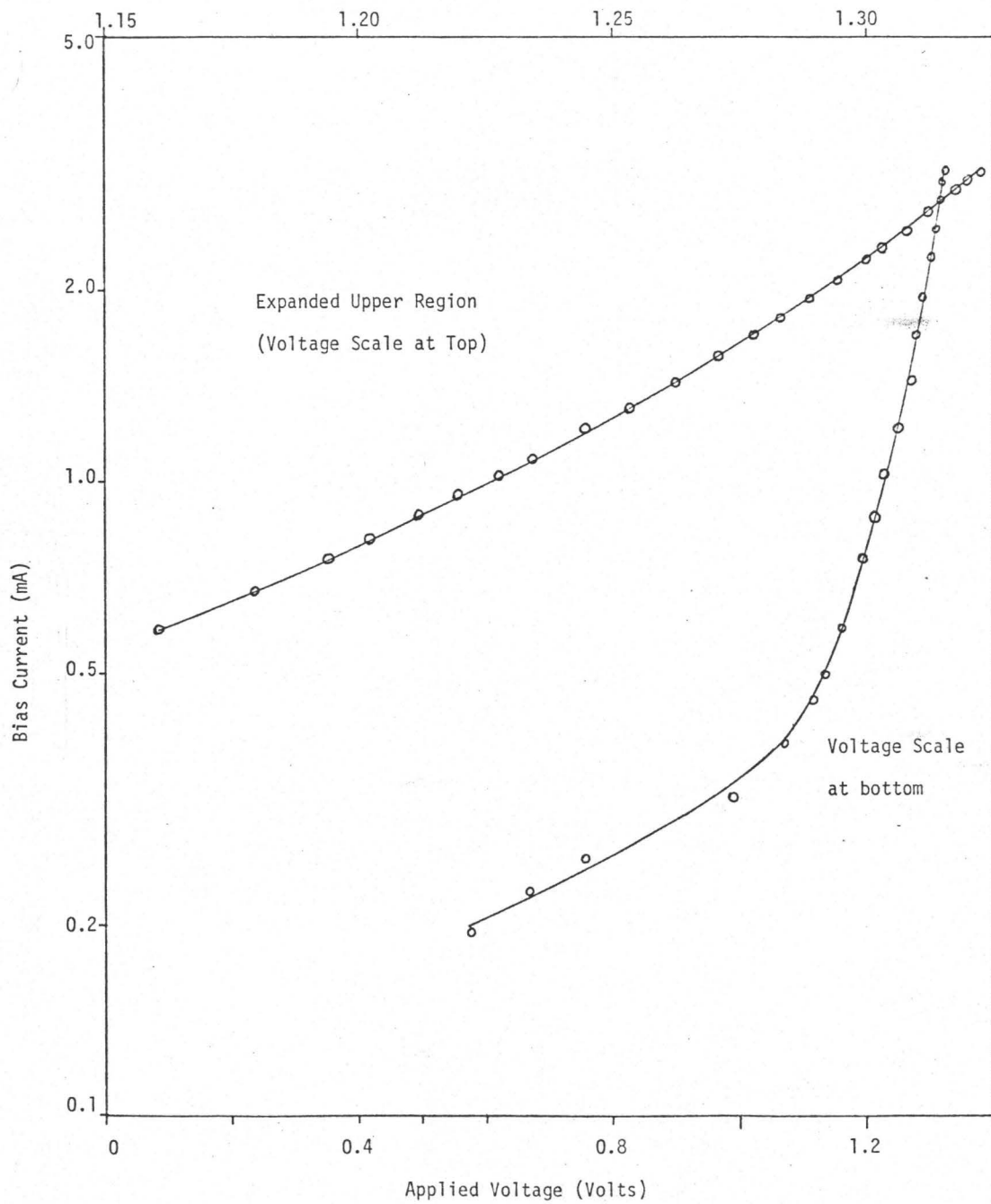


Figure 10 I-V Characteristics of LED 42/45

Figure 10 shows the I-V data for LED 42/45. If I was proportional to  $\exp(qV/nkT)$ , we would expect a straight line with slope corresponding to  $q/nkT$ . As the plot shows, there are two approximately straight line sections of considerably different slopes. These slopes differ by a factor of about eight. This is much more than can be accounted for by the factor of 2 difference in "n" between the low current junction theory and the high current theory.

It was also suggested that the shape of the plot may be accounted for by a significant IR drop across the device's bulk resistance at high currents. As will be shown later, the bulk resistance is expected to be less than  $5 \Omega$ . Currents of the magnitude shown in the plot would not have caused so large a jog in the curve. As well, a significant IR drop would have caused a smaller slope at high  $I_{DC}$ , not a larger one.

It is thought that the low current segment corresponds to the  $I_{DC}$  range where the current is distributed over the entire area of the chips. The steeper high current region would then correspond to the size of the working junction being of the same order as the contact through the oxide layer. The intermediate "elbow" region would be where the junction size is changing rapidly with  $I_{DC}$ . If this explanation is accepted for now, then it can be seen from the slight upward curvature of the expanded upper region of Figure 10 that the junction size is still changing.

According to the theory outlined in Sze, at low frequencies ( $\omega\tau \ll 1$ ), the quantity  $R_p C_{diff}$  should be constant with  $\omega$ ,  $I_{DC}$ .

If  $\tau$  is of the order of 2 ns, then  $\omega = 1/\tau$  corresponds to  $f = 80$  MHz.

It is obvious that over the frequency range of interest in the impedance runs,  $R_p C_{diff.}$  would not be constant with  $\omega$ . However,  $R_p C_{diff.}$  should still be constant with  $I_{DC}$ .

### 3.2 Analysis of data

When the first attempt was made to fit the impedance expression (2) to the 4815A curves, it became obvious that the calculated values of capacitance were very sensitive to errors in  $R_s$ ,  $R_p$  and  $L$ . To correct this, a 500 kHz run was done on 42/45 with the impedance meter. It was thought that the effect of  $L$  and  $C$  could be ignored at this frequency and so the measured impedance would then just be  $R_s + R_p$ . Hopefully, this data will yield a more accurate value for  $R_p$  than was possible with just the I-V curve of the device.

Even if we simply take  $|Z| = R_s + R_p$ , it must still be decided what the individual  $R_s$  and  $R_p$  values are. The obvious way to do this is to go to **very** high  $I_{DC}$  such that  $R_p \ll R_s$ , and then take  $R_s = |Z|$  there. At  $I_{DC} = 50$  mA,  $|Z|$  is less than six ohms, but still decreasing significantly. This at least puts an upper bound on  $R_s$ . Because of heat sinking difficulties, currents above 50 mA were not used.

It should be pointed out that no external method can be used to measure  $R_s$ . The value of  $R_s$  that is finally determined must somehow come from the impedance readings of the device as it is connected to the impedance meter probe. The reason for this is that the resistance of the contacts must be accounted for.

To determine  $R_S$ , an iterative method was used. This consists of first making an educated guess at an  $R_S$  value, then subtracting it, plus  $0.5 \Omega$  due to probe, from the  $|Z|$  measurements at high  $I_{DC}$  in the 500 kHz run. The remaining quantity should then be  $R_p$ . Assuming that  $R_p$  is proportional to  $(I_{DC})^{-1}$  in this high  $I_{DC}$  range, these  $R_p$  values are plotted against  $I_{DC}$  in a semi-log plot. The reasoning is that if the correct value of  $R_S$  is chosen, the difference will be exactly  $R_p$  and the plot should show a straight line. This was done for  $|Z|$  measurements taken at  $I_{DC} = 30$  mA and over. Reasonably straight lines were found for  $R_S$  values just under  $4 \Omega$ . The value  $R_S = 3.8 \Omega \pm 0.4 \Omega$  was chosen as a first approximation. If the effect of the probe is not exactly  $0.5 \Omega$ , the difference will be taken up in  $R_S$ .

At this point, several intermediate steps are needed before the second iteration for  $R_S$  can be done.

Where the phase angle of the impedance curves goes through zero, the imaginary component of the impedance expression is zero. If this is true, then the measured  $|Z|$  is equal to the real component alone, i.e.

$$|Z| = (R_S + 0.5 \Omega) + \frac{R_p}{1 + (\omega R_p C)^2}$$

At this point, we have the  $R_S$  and  $R_p$  values. Knowing  $|Z|$  at the phase zeroes, we can determine  $C$ . The data obtained from the phase zeroes of LED 42/45 in the low inductance configuration is tabulated below.

TABLE I

Zero Phase Information for LED 42/45 (taking  $R_3 = 3.8 \Omega$ )

Frequency of Run (MHz)	$I_{DC}$ of phase zero (mA)	Measured $ Z $ at phase zero	$R_p$	$(\omega R_p C)^2$	$R_p C$ (ns.)	C
40	3.30	5.8 $\Omega$	17.7 $\Omega$	10.8	13.1	740 pf
60	1.98	6.1	30.3	15.8	10.5	347
80	1.42	6.6	45.4	18.7	8.6	189
100	1.10	6.9	58.0	21.3	7.3	127

The  $R_p$  values were calculated from the 500 kHz run, taking  $R_s = 3.8 \Omega$ .

From the impedance expression, we see that at the phase zeroes we have:

$$\omega L - \frac{\omega R_p^2 C}{1 + (\omega R_p C)^2} = 0$$

Since we now have the capacitance values at the phase zeroes, we can calculate L. Inductance values calculated in this manner for each of the phase zeroes are tabulated below.

TABLE II

Inductance Values Calculated from Phase Zero Information for LED 42/45 (with  $R_s = 3.8 \Omega$ )

Frequency of Run (MHz)	Calculated Inductance (nH)
40	19.7
60	18.9
80	19.8
100	19.0
L average = 19.4 nH	

These inductance values will include the 8 nH due to the impedance meter probe.

Now a technique is required for determining  $C$  at  $I_{DC}$  values other than those of the phase zeroes. Since we have fairly trustworthy values for  $R_S$  and  $L$ , we could calculate  $C$  from either the real component or the imaginary component of the impedance. To check the reliability of the calculations, capacitance values will be calculated from both components. Hopefully the impedance expression will hold true and the two calculated capacitance values will be similar.

The magnitudes of the real and the imaginary components of the impedance were calculated from the measured values of  $|Z|$  and  $\theta$ . These values were set equal to the real and imaginary components of the impedance expression. Knowing  $L$  and  $R_S$ , the capacitances are calculated for both components. Figure 11 shows the results of these calculations done on the data from various runs.

During the course of these calculations, it was realized that the inaccuracy in the  $R_S$  value that is being used could lead to an appreciable inaccuracy in the resulting capacitance values. For this reason, a second iteration to get a more accurate  $R_S$  value would be very useful.

At  $I_{DC} = 50$  mA, we expect  $R_p$  to be very small. By considering the real components of the impedance at this current, we can get a more accurate value of  $R_S$ . The real components of the impedance at 50 mA drop appreciably as the frequency increases. This behaviour roughly fits that predicted by expression (2). At 100 MHz, the real

Figure 11

Calculated Capacitance of LED 42/45

Calculated Capacitance (pf)

- + capacitance calculated from real component of impedance
- capacitance calculated from imaginary component of impedance

20 MHz

40 MHz

80 MHz

0

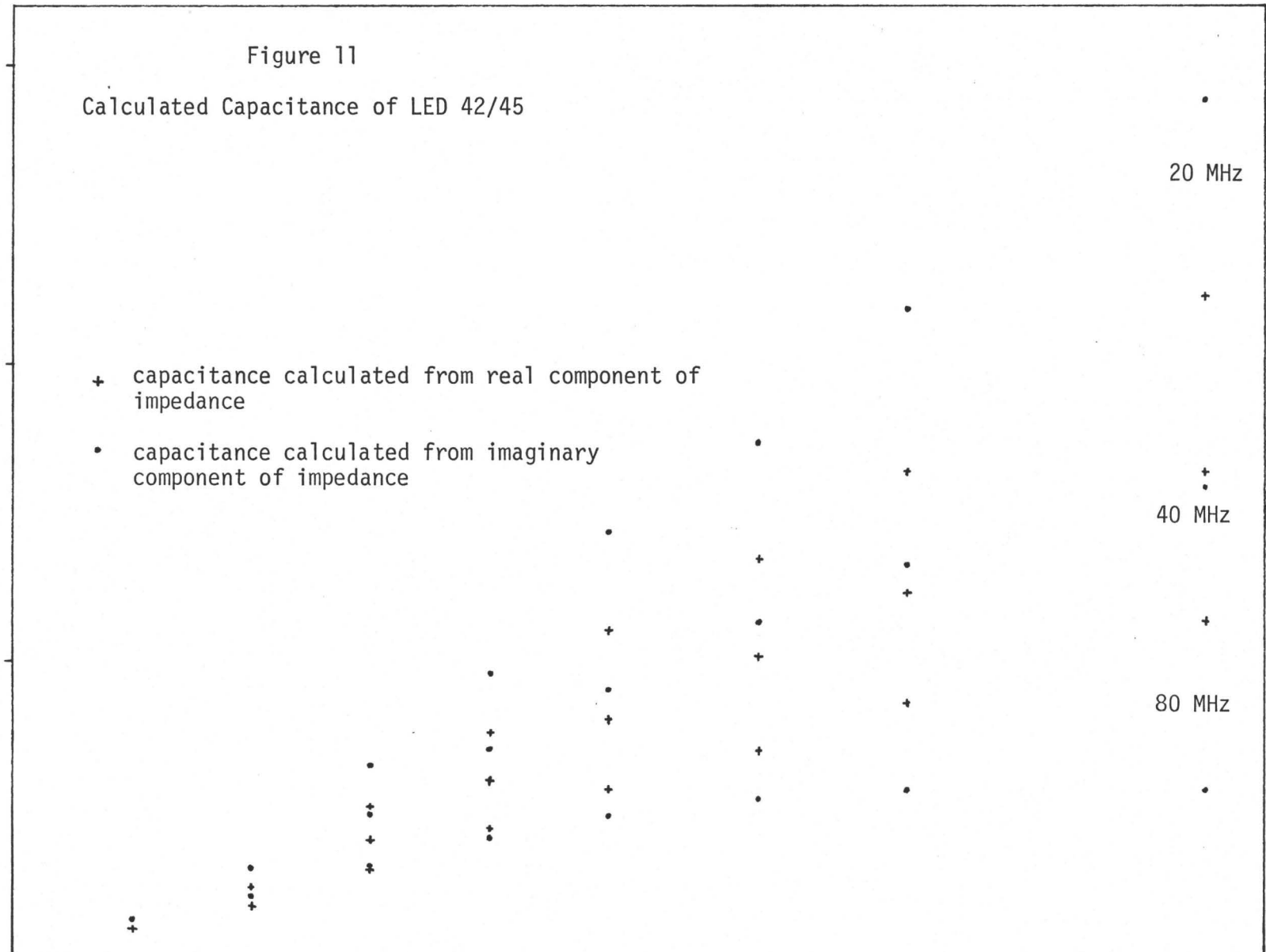
1.0

2.0

3.0

4.0

$I_{DC}$  (mA)



component  $|Z| \cos \theta = 4.17 \Omega$  at 50 mA. At 500 kHz,  $|Z| \cos \theta = 5.6 \Omega$  at 50 mA. At 500 kHz, we can safely say  $(\omega R_p C)^2 \ll 1$ , and so  $R_s + R_p + 0.5 \Omega = 5.6 \Omega$ . Taking our first approximation of  $R_s = 3.8 \Omega$ , we get  $R_p = 1.3 \Omega$  at 50 mA. From TABLE I, we know that  $(\omega R_p C)^2 = 21.3$  for the 100 MHz run, at the zero phase  $I_{DC}$ . If this quantity is approximately constant with  $I_{DC}$ , we have

$$\frac{R_p}{1 + (\omega R_p C)^2} = \frac{1.3 \Omega}{22.3} = 0.06 \Omega \quad \text{at 100 MHz, 50 mA}$$

This is such a small quantity that we can safely say  $R_s = 4.17 \Omega - 0.06 \Omega - 0.5 \Omega = 3.6 \Omega$ , using the 100 MHz figures. Due to inaccuracies in the measured quantities, this value of  $R_s$  is probably good to within about  $0.2 \Omega$ .

The tables below are similar to I and II, except that now the quantities are calculated using  $R_s = 3.6 \Omega$ .

TABLE III

Zero Phase Information for LED 42/45 (taking  $R_s = 3.6 \Omega$ )

Frequency of Run (MHz)	$I_{DC}$ of phase zero (mA)	Measured $ Z $ at phase zero	$R_p$	$(\omega R_p C)^2$	$R_p C$ (ns.)	C
40	3.30	5.8 $\Omega$	17.9 $\Omega$	9.5	12.3	686 pf
60	1.98	6.1	30.5	14.3	10.0	328
80	1.42	6.6	45.6	17.2	8.26	181
100	1.10	6.9	58.2	19.8	7.08	122

TABLE IV

Inductance values Calculated From Phase Zero Information for LED 42/45  
(with  $R_S = 3.6 \Omega$ )

Frequency of Run (MHz)	Calculated Inductance (nH)	
40	20.9	
60	20.0	
80	20.7	
100	19.8	L average = 20.3 nH

These last values of  $R_S$  and  $L$  are the values which were used in calculating the capacitances plotted in Figure 11.

### 3.3 Discussion of Capacitance Measurements

As can be seen from Figure 11, there is considerable disagreement between the capacitances calculated from the real component of the impedance and those calculated from the imaginary component. However, the general trend is as we expect for diffusion capacitance - it increases with  $I_{DC}$  and decreases with frequency. In first order, an inaccurate value for  $R_S$  would affect only the real component of the impedance and  $L_{stray}$  would affect only the imaginary component. In view of this, the capacitances were re-calculated for slightly different values of  $R_S$  and  $L_{stray}$  than were used for the plotted points.

The parameter  $L_{stray}$  was varied between the extremes of the calculated values, i.e. between 19.8 nH and 20.9 nH. The resulting capacitances were only affected by about one percent or so - much less

than the observed discrepancy. As expected, the effect of  $L_{\text{stray}}$  is a maximum at high frequencies and high  $I_{\text{DC}}$ , where the inductive reactance makes a larger fraction of the total impedance. Obviously, the discrepancies shown in the plot are due to something other than an incorrect inductance value.

Varying the parameter  $R_s$  in the range  $R_s = 3.6 \Omega \pm 0.2 \Omega$  had a larger effect. As would be expected, this was largest at high  $I_{\text{DC}}$ . In some cases, the effect of  $R_s$  is enough to account for the difference between the two calculated capacitances. However, no consistent "proper" value of  $R_s$  is favoured for all  $I_{\text{DC}}$  and all frequencies.

The most likely cause of the poor fit of the calculated capacitances to the impedance expression is the fact that a discrete component model was used, rather than a more realistic distributed model.

## CHAPTER 4

### RADIO FREQUENCY VECTOR DRIVE EFFICIENCY EXPERIMENT

#### 4.1 Theory and Experimental Procedure

There was concern over what fraction of the current that is observed with the current probe actually goes into building the population inversion at the start of a pulse. For instance, the large (order of 200 pf) capacitance that is observed in oxide stripe lasers at zero bias can be expected to shunt the higher frequency components of a fast current pulse that is applied to the device. This shunting effect would mean that the shape of the injection current pulse is more slowly rising and falling than the external current pulse. This would change the time delay expression, even beyond any calculations that could be done after accounting for the finite risetime of the external current pulse. If series inductance further complicates the problem, it is difficult to predict how the inversion builds up in time.

To investigate what happens to the various frequency components at different DC biases, it was decided to set up an experiment to measure the R.F. drive efficiency at low DC biases. We know from the impedance results that the series resonances for frequencies under 100 MHz occur for  $I_{DC}$  above 1 mA. As  $I_{DC}$  increases, and the junction size decreases, we expect the "dead layer" capacitance to drop as well, since less of the chip becomes accessible to the current. From

the I-V plot of LED 42/45, we expect this to occur for  $I_{DC} < 0.5$  mA. Information on the drive efficiency at various frequencies, over these two current ranges, could prove very useful in explaining some of the time delay behaviour.

This drive efficiency experiment could prove useful for another reason. If  $\tau$  is on the order of 2 ns, and the light emitted has a frequency dependence like  $n/(1 + j\omega\tau)$  where  $n$  is the injection electron density, then it may be possible to determine  $\tau$  from the phase change between the received light and the applied RF current. This would be another, independent method for pointing out how  $I_{DC}$  affects the  $\tau_{sp}$  value, as measured by the time delay method.

On performing the experiment, we would like to have fairly good resolution of the drive efficiency as a function of  $I_{DC}$ . This limits the RF peak-to-peak amplitude to be less than 10% or so of  $I_{DC}$ . With this in mind, and assuming the RF drive efficiencies to be of the same order as at DC, a rough calculation shows that the photo-signal from an avalanche photo-diode at reasonable gain will not be large enough to be displayed on an oscilloscope. Some sort of amplification would be needed after the APD for this to be done.

Other than the sensitivity consideration just mentioned, another constraint on the photo-detection system is that it should not lose the phase information if we expect to be able to determine  $\tau$ . For this reason, a photo-multiplier tube cannot be used to solve the sensitivity problem.

A fast avalanche photo-diode could be used to produce a reasonably large photo-signal that is phase consistent with the received

light. It would be best to avoid using an external amplifier after the APD, before the signal is displayed. Such an amplifier could be expected to produce phase changes that are a function of frequency, and possibly of amplitude and source impedance as well. This phase change could conceivably be calibrated over the expected range of operating conditions, but it would be tedious.

The photo-signal from an APD could be enhanced in a phase consistent manner simply by increasing the load resistor from  $50 \Omega$ . It would then be necessary to use some sort of high impedance probe to carry the signal. At any frequency, the load resistor value is limited by the stray capacitance across it, and the device capacitance. With some of the smaller, low capacitance APD's that are available, i.e. TIXL55, it may be possible to have the 3 db point at 100 MHz with a load resistance of on the order of  $500 \Omega$ . Such a tenfold enhancement would be a great help in boosting the low signal levels that can be expected from this drive efficiency experiment.

Increasing the gain of the APD is another obvious means of enhancing the signal. The limit to the gain is when the DC photo signal approaches the power rating of the device. For  $I_{DC}$  in the range of interest, this limits the gain to the order of ten or so.

To display both the magnitude of the received light, and the phase angle with respect to some reference signal, a vector voltmeter could be used. An HP8405A, operating in the range of 1-1000 MHz was available. Its most sensitive magnitude scale is 0.1 mV full scale, which should be sufficient for the expect photo-signals. The most sensitive phase scale is  $\pm 6^\circ$  about an adjustable offset.

For a sweep in  $I_{DC}$  up to 5 mA, an RF current amplitude of 0.1 mA p-p would be a reasonable compromise between resolution and signal strength. To observe only the magnitude of the drive efficiency vs  $I_{DC}$ , a cooled photo multiplier tube was used as the detector. This was followed by an amplifier, and the amplified signal was displayed on an oscilloscope. The displayed signal was then large enough to measure easily. The trace seemed to be slightly smeared along the time axis. The oscilloscope was then replaced by the vector voltmeter, using the RF drive current signal as a reference. The voltmeter's magnitude meter reading was erratic, and the phase reading even more so. The smearing effect of the photo-signal was thought to be due to the differential delay of the electrons in the photo-multiplier tube. Since the vector voltmeter operates by sampling the incident signal, the spread in delay time could cause an ambiguous phase relationship with the reference. A similar effect in photo-diodes would be due to a finite transit time. This was kept in mind when selecting the detector that was eventually used.

An RCA 30902E avalanche photo-diode was used as the detector. It has a small capacitance of the order of 2 pf under high reverse bias, and this capacitance varies slowly with bias in the high gain region. The vector voltmeter probe will be across the load resistor during the course of the experiment. According to the manual, it would add 2.5 pf to the shunt capacitance. When the detection circuit was completed, a load resistor of 270  $\Omega$  was installed. The total measured capacitance across the load was 5.5 pf at 150 v reverse bias.

To supply the necessary signals to the voltmeter, the RF drive was sent into a TEE junction. One arm of the TEE consisted of a  $50 \Omega$  termination, across which the voltmeters reference signal was taken. The other arm held the drive circuit and DC biasing network. A drive efficiency run consisted of two individual runs. The first run was done with the voltmeters signal probe across the output of a current probe which was in series with the LED. The recorded data of this run then consisted of two X-Y plots. One was of the RF current magnitude vs  $I_{DC}$ , at a fixed frequency. The second was of the phase difference between the RF drive current and the reference signal, as a function of  $I_{DC}$ . The second run was done with the signal probe across the load resistor of the detection circuit. Again, two X-Y plots were produced. One was of the photo-signal magnitude vs  $I_{DC}$ . The second plot was of the phase difference between the reference signal and the photo-signal. This second, photo-signal run was done under the same conditions as the drive current run. By analyzing the data from both runs, the necessary phase and magnitude information concerning the drive efficiency could be found.

#### 4.2 Discussion of RF drive efficiency results

Due to time limitations, the data recorded from drive efficiency runs on LED 42/45 was of a crude, qualitative nature. However, some general trends were noticed:

- drive efficiency decreases with frequency; this is to be expected if injection-shunting capacitance is present and if  $1/\tau$  is much less than the frequencies

being used.

- at all frequencies, the drive efficiency is low until the DC bias is about 0.5 mA.
- no significant structure is found in the drive efficiency at  $I_{DC} > 1$  mA, however the impedance bellies of LED 42/45 in the mount for the drive efficiency experiment were very shallow.

If accurate, reliable data had been taken, it would in theory be possible to obtain a value for the spontaneous carrier lifetime from the phase or magnitude relationship of the drive efficiency. However, to analyze the data, it is necessary to know the density of injected carriers as a function of distance from the junction and to know the time it takes the carriers to reach a given distance from the junction. This information was not available at the time.

## CHAPTER 5

### CONCLUSIONS

It was observed that the spontaneous carrier lifetime, as measured by the time delay method, is very sensitive to small DC biases of the injection laser. The measured lifetime goes to a pronounced minimum at a critical value of the DC bias. There is evidence to suggest that at this critical  $I_{DC}$ , there is a series resonance at some component frequency of the rising side of the drive pulse between the stray series inductance and the DC bias dependent device capacitance.

Since the shape of the external current pulse does not change significantly near the critical DC bias, the resonance must influence the efficiency at which the applied current pulse appears as injected carriers. The most likely mechanism for this is that the effect of injection-shunting capacitance is minimized at the series resonance. If this is true, it is reasonable to conclude that the lifetimes measured by the time delay method are always larger than the actual value, and approach it only at the critical bias where the measured lifetime is a minimum. This mechanism would also explain the low drive efficiencies at  $I_{DC} < 0.5$  mA. For LED 42/45, the working junction is very large in this bias range, and so the injection shunting capacitance is expected to be large.

The R.F. impedance measurements are a useful method of determining the capacitance under forward bias. However, the measured capacitances do not satisfactorily fit to the impedance expression derived for the equivalent circuit model. This is probably due to the simplicity

of the model. A model based on distributed parameters would be much closer to reality, especially in view of the changing junction size. Proton bombarded devices may perhaps fit well to a discrete component model. Such devices would be better suited to most of these experiments because of their constant junction size, constant  $R_s$ , etc. At any rate, the measured capacitances become quite large with  $I_{DC}$ . Since this is due to diffusion capacitance of carriers that have already been injected, it doesn't seem to affect the drive efficiency.

Neither of the alternative methods of determining the spontaneous carrier lifetime proved satisfactory. Again, the problems that were encountered suggest that proton-bombarded devices would be considerably easier to analyze than the oxide stripe devices that were used.

#### REFERENCES

- [1] J.E. Ripper, J. Appl. Phys., 43, 1762 (1972).
- [2] S.M. Sze, "Physics of Semiconductor Devices", Wiley and Sons, 1969.
- [3] T.P. Lee, Bell Sys. Tech. Journal, Vol. 54, #1, 53.